Curvature, torsion, microcanonical density and stochastic transition

1996 J. Phys. A: Math. Gen. 29 3733

(http://iopscience.iop.org/0305-4470/29/14/003)

J. Phys. A: Math. Gen. **29** (1996) 3733–3747. Printed in the UK

Curvature, torsion, microcanonical density and stochastic transition

Carlo Alabiso†‡, Nicola Besagni†, Mario Casartelli†§ and Paolo Marenzoni‖

† Dipartimento di Fisica dell'Università di Parma, I-43100 Parma, Italy
‡ INFN, Gruppo collegato di Parma, Italy
§ INFM, Parma, Italy
‖ Dipartimento di Ingegneria dell'Informazione dell'Università di Parma, Italy

Received 19 December 1995, in final form 9 April 1996

Abstract. We introduce geometrical indicators (Frenet–Serret curvature and torsion) together with microcanonical density to give evidence to the stochastic transition of classical Hamiltonian models (Fermi–Pasta–Ulam and Lennard–Jones systems) when the specific energy grows. The transition is clearly detected through the breakdown of the harmonic-like behaviour, in combination with the vanishing of the dependence on the initial conditions. This method of analysis presents both experimental and theoretical advantages: it is fast and gives relatively sharp answers for the transition; moreover, a new insight is allowed on the deformations and the destruction of invariant surfaces in the ordered regime. Among the results, it is noteworthy that going from 32 to 4096 degrees of freedom the stochastic transition depends only on the specific energy and not on the number of degrees of freedom.

1. Introduction

To detect the transition from an ordered to a chaotic regime of motion, dynamical observables sensitive to the different features of trajectories are required. The evaluation of the Lyapunov exponents, for example, is a direct method, based on the uncorrelation rate of nearby starting orbits [1]. Being related to Kolmogorov entropy, Lyapunov exponents admit a precise interpretation in terms of statistical properties. We note however that their computation requires a double integration of the equations of motion and that, moreover, 'null' Lyapunov exponents do not appear as such in numerical simulations. Other (non-direct) methods are the equipartition based criteria, which exploit the statistical consequences of disorder. Some critical features of the latters, with a special reference to the stochastic regime of motion and to the thermodynamic limit, are discussed in [2, 3]. (See also [4] and [5] for recent results on the relations between time scales and number of degrees of freedom for transition criteria based on equipartition.) In both cases, Lyapunov and equipartition based indicators, the crossover between ordered and disordered regions is sometimes difficult to appreciate, because of the long time scales in the approach to equilibrium.

The main practical advantage of the method introduced here is that such a crossover is particularly neat and fast to estimate. In fact the scanning in the order parameter (say, the energy) does not require, as is usual with other indicators, a particularly good relaxation. Actually, our indicators are based on observables, both 'geometrical' (curvature, torsion) and dynamical (microcanonical density), which show a sharp breakdown of quasi-harmonicity. Such a breakdown, sufficient to distinguish two regimes of motion, occurs very early in time

0305-4470/96/143733+15$19.50

and is extremely stable. After localization of the critical value of the order parameter, a few experiments are sufficient to test the possible vanishing dependence on the initial conditions, as suggested by the Birkhoff theorem, in order to establish a connection between the quasi-harmonicity breakdown and the onset of stochasticity. Of course, those few checks require, in general, the long relaxation times already known through other methods.

The features we are interested in (i.e. stochasticity or quasi-integrability) are intrinsic of the system and do not depend on the coordinates. On the other hand, the indicators may be different for different coordinate systems, since they are only required to be effective in emphasizing what we are looking for. Therefore, it is totally irrelevant that observables such as curvature or torsion are not canonically invariant. The same happens, for example, for equipartition based criteria, where normal modes are not interchangeable with arbitrary coordinates.

On the background, there is the possible link between the 'geometry of order and chaos', as suggested by the KAM theory, and the properties of the trajectories. The stochastic transition, whose very definition is far from being clear and universal, is involved in such an analysis in a natural way, to the extent that it gives a plausible picture of the invariant surface deformation process in the ordered region. In other terms, since the transition from quasi-integrability to chaoticty is characterized by the progressive vanishing of invariant surfaces, which act as local geometrical constraints, the present approach gives direct insight into the structural features of the dynamical system.

To avoid any misunderstanding, we recall that there is a widely shared opinion (see [6] and references therein) about the persistence of stochasticity even at very low energy, with the following features: a diffusion motion which takes exponentially longer and longer times to reach the equilibrium, and the practical disappearance, at growing N, of quasi-integrability in the strict KAM sense. According to this opinion the onset of stochasticity discussed throughout the present paper has to be recognized as the 'strong stochastic transition' (SST), i.e. the transition from weak to strong stochasticity, and not from quasi-integrability to stochasticity. We do not discuss this point here: when speaking of ordered and disordered regions we keep a phenomenological attitude, by distinguishing (if possible) only the qualitative behaviour of the systems. Thus, below threshold, the quasi-harmonicity (i.e. time averages keeping the values of the harmonic system with the same initial conditions) is compatible, in principle, with both the possibilities: the weak stochasticity quoted above and the quasi-integrability in the KAM sense. We assume the last conceptual frame because it suits the existence of local geometrical constraints, strongly supported by our simulations. It is only in this sense, and not in relation to the rigorous methods of the classical perturbation theory, that we use terms like 'ordered motion' and 'quasi-integrability'.

Tentative experiments, based on the Frenet–Serret curvature along the orbit and microcanonical density, partially developed these ideas in [7]. The main goal there was to compare the behaviour of indicators based on the previous quantities with the rate of energy exchanges, in order to give evidence to trapping phenomena in the weakly stochastic domain. Returning to this item here, we exploit computational improvements, a better choice and definition of the geometrical observables, and a clearer understanding of their relation with the structure of the ordered region.

The main result is the particularly clear evidence that the quasi-harmonic, anharmonic or stochastic behaviours depend on the specific energy only, and consequently that the thresholds are independent of N. This fact constitutes a strong indication on the persistence of ordered motion in the thermodynamic limit.

An alternative geometrical approach to the same problems has been developed in a

series of papers [8–10] using concepts and tools taken from the Riemannian geometry of manifolds. They explore proper sources of stochasticity, such as the existence of subdomains with negative curvature, and the parametric resonance induced by fluctuations of Ricci curvature, independently of negativeness. This approach proves very fruitful, leading to a rich set of results which, as far as they can be matched, are in excellent agreement with ours, in particular with those referring to the thermodynamic limit.

The connections between these two geometrical methods seem possible, in principle, but hard to establish. Each of them presents some advantage with respect to the other, with a certain degree of complementarity. Generally speaking, the very nature (or existence) of weak chaos could be involved, but direct comparisons are difficult even on the grounds of numerical simulations. For the moment, besides the particular simplicity of the mathematical apparatus required by our method, we stress the advantage of easy insight into phase space, whose geometrical structure below threshold is naturally inspected by our observables. Moreover, even with respect to the other geometrical approach, we claim the convenience of dealing with the quasi-harmonicity phenomenon, which requires in principle shorter times of relaxation. However, we lack explicit comparisons.

Numerical simulations regard the classical Fermi–Pasta–Ulam (FPU) and Lennard–Jones (LJ) models, with suitable variations (e.g. of the boundary conditions) to study the role and the influence of various parameters. The Toda model is also considered for comparison with an integrable system: for this model too, a transition from quasi-harmonic to non-harmonic behaviour may be easily established. In this case, however, a stable dependence on initial conditions holds for all the values of the parameters below and above this threshold which, therefore, does not indicate any stochastic transition.

2. Geometric features of trajectories in phase space

In the standard terminology of curves in $\boldsymbol{R}^3$, where the tangent versor $\boldsymbol{t}$, the principal normal $\boldsymbol{n}$ and the binormal $\boldsymbol{b}$ are well defined quantities, the Frenet–Serret (FS) formulae are:

$$\frac{\mathrm{d}\boldsymbol{t}}{\mathrm{d}s} = \kappa\boldsymbol{n} \qquad \frac{\mathrm{d}\boldsymbol{n}}{\mathrm{d}s} = -\kappa\boldsymbol{t} + \tau\boldsymbol{b} \qquad \frac{\mathrm{d}\boldsymbol{b}}{\mathrm{d}s} = -\tau\boldsymbol{n}. \tag{1}$$

The variation of the tangent versor defines the first curvature κ (or 'curvature' *tout court*). This quantity represents the inverse radius of the osculating circle in the plane $(\boldsymbol{t}, \boldsymbol{n})$, and it is positive definite. The component of the variations of the reference versors of the osculating plane outside the plane itself, i.e. the vector $\tau\boldsymbol{b}$ as read in the second FS formula, defines the second curvature τ (or 'torsion'), which is not a positive definite quantity. Note that the third formula also defines the torsion, via the variation of the binormal.

Going from $\boldsymbol{R}^3$ to $\boldsymbol{R}^N$ [11] the first two equations do not change. Therefore, these can be used to directly define curvature and torsion for curves in $\boldsymbol{R}^N$, whereas the third equation requires a generalization that includes a third curvature (actually, the number of equations rises to N, with $N-1$ curvatures).

The curves we consider are trajectories in the $2N$-dimensional phase space of a classical Hamiltonian system, with N degrees of freedom and homogeneous canonical coordinates $(\boldsymbol{p}, \boldsymbol{q})$. With these variables the infinitesimal arc of trajectory is given by

$$\mathrm{d}s = \left(\sum_{i=1}^{N} (\mathrm{d}p_i^2 + \mathrm{d}q_i^2) \right)^{1/2}$$

and the tangent versor by

$$\boldsymbol{t} = \{\mathrm{d}p_1/\mathrm{d}s, \ldots, \mathrm{d}p_N/\mathrm{d}s, \mathrm{d}q_1/\mathrm{d}s, \ldots, \mathrm{d}q_N/\mathrm{d}s\}.$$

Note that in the harmonic case the energy of the kth oscillator is $E_k = \frac{1}{2}\omega_k(p_k^2 + q_k^2)$, so that the harmonic torus is the product of exact circles, whose curvatures are constants of motion depending on the distribution of energies among the normal modes. The explicit formula for the harmonic curvature is given in section 3.

For every quantity f, the objects of actual computations are time averages and variances along the orbit up to the time T, i.e.

$$\langle f\rangle = \frac{1}{T}\int_0^T f(\boldsymbol{p}(t), \boldsymbol{q}(t))\,\mathrm{d}t \qquad \mathrm{Var}(f) = \frac{\langle f^2\rangle - \langle f\rangle^2}{\langle f\rangle^2}. \tag{2}$$

For simplicity we omit the T dependence.

The variances give an estimate of the dispersion around the mean value. They are identically 0 for harmonic oscillators, but meaningful, in principle, for anharmonic systems.

We use the following geometrical quantities:

- the curvature, as defined through the first equation in (1),
- the absolute value of torsion, as defined through the second equation in (1),
- the absolute value of the derivative of curvature and torsion.

From the combined analysis of averaged values and variances of these, one can draw non-trivial consequences about the invariant surfaces deformation.

Besides the geometrical quantities, we also make use of the microcanonical density

$$\rho = \frac{1}{|\nabla H(\boldsymbol{p}, \boldsymbol{q})|} = \frac{1}{|\boldsymbol{v}|} = \frac{\mathrm{d}t}{\mathrm{d}s} \tag{3}$$

which is a well defined observable, independent of the ergodicity of the system. It has the meaning of 'sojourn time'.

In the harmonic case, all the three quantities ρ, κ and τ are constant of motion and proportional to $E^{-1/2}$, as deduced from the explicit expression (see section 3). Therefore, in order to give more evidence to the departure from the harmonic behaviour, we also plot 'normalized quantities':

$$\langle\rho\rangle_n = A\frac{\langle\rho\rangle}{E^{-1/2}} \tag{4}$$

with the numerical factor A chosen for graphical convenience, and

$$\langle\kappa\rangle_n = \frac{\langle\kappa\rangle}{\langle\rho\rangle} \qquad \langle|\tau|\rangle_n = \frac{\langle|\tau|\rangle}{\langle\rho\rangle}. \tag{5}$$

This last normalization through the microcanonical density is justified by two facts: first, in the quasi-harmonic regime it gives the same effect as the normalization through $E^{-1/2}$; second, in the anharmonic regime, the energy surface becomes more complicated than the harmonic surface at the same energy, which implies, on one side, a relative increase of the mean curvature and torsion and, on the other side, a relative reduction of the mean density, i.e. of the microcanonical density. Therefore, this normalization is expected to amplify the anharmonic deviation of averaged curvature and torsion.

3. Models

The harmonic Lagrangian, with periodic boundary conditions ($x_1 \equiv x_{N+1}$), is

$$\mathcal{L}_0(\boldsymbol{x}) = K - \chi V_2 = \frac{1}{2}\sum_{i=1}^{N}\dot{x}_i^2 - \frac{\chi}{2}\sum_{i=1}^{N}(x_i - x_{i+1})^2. \tag{6}$$

The diagonalization is obtained in the standard canonical coordinates $\{\hat{\boldsymbol{p}}, \hat{\boldsymbol{q}}\}$ correlated to Lagrangian coordinates $\{\dot{\boldsymbol{x}}, \boldsymbol{x}\}$ by $\dot{\boldsymbol{x}} = \boldsymbol{B}\hat{\boldsymbol{p}}$, $\boldsymbol{x} = \boldsymbol{B}\hat{\boldsymbol{q}}$, with the unitary matrix $\boldsymbol{B} = \{\beta_{i,k}\}$ given by

$$\begin{cases} \beta_{i,k} = \sqrt{\dfrac{2}{N}} C_k \cos \dfrac{(2(k-1)\mathrm{i}\pi)}{N} & k = 1, \ldots, M \\ \beta_{i,k} = \sqrt{\dfrac{2}{N}} C_k \sin \dfrac{(2(N-k+1)\mathrm{i}\pi)}{N} & k = M+1, \ldots, N \end{cases} \tag{7}$$

with $M = [N/2] + 1$, where $[N/2]$ is the integer part of $N/2$. The resulting harmonic spectrum is twofold degenerate:

$$\omega_k = 2\sqrt{\chi} \sin \frac{((k-1)\pi)}{N}. \tag{8}$$

With fixed boundary conditions, ($x_0 \equiv x_{N+1} = 0$), the second sum in the Lagrangian (6) starts from $i = 0$, while the matrix $\boldsymbol{B}$ reads

$$\beta_{i,k} = \sqrt{\frac{2}{N+1}} \sin \frac{\mathrm{i}k\pi}{N+1} \tag{9}$$

and the harmonic spectrum is non-degenerate:

$$\omega_k = 2\sqrt{\chi} \sin \frac{k\pi}{2(N+1)}. \tag{10}$$

By introducing the homogeneous coordinates

$$p_k = \hat{p}_k/\sqrt{\omega_k} \qquad q_k = \hat{q}_k\sqrt{\omega_k}$$

in both cases the harmonic Hamiltonian reads

$$H_0(\boldsymbol{p}, \boldsymbol{q}) = \tfrac{1}{2}\sum_{k=1}^{N} \omega_k (p_k^2 + q_k^2) = \sum_{k=1}^{N} E_k = \sum_{k=1}^{N} \omega_k J_k \tag{11}$$

where E_k are the harmonic energies and J_k the action variables. With periodic boundary conditions, $\omega_1 = 0$ and J_1 is not defined. The missing degree of freedom corresponds in this case to the translational invariance of the Hamiltonian.

In the harmonic model, microcanonical density, curvature and torsion assume the following explicit form:

$$\begin{aligned} \rho &= \left(2\sum_k \omega_k E_k\right)^{-1/2} \\ \kappa &= \rho^2 \left(2\sum_k \omega_k^3 E_k\right)^{1/2} \\ |\tau| &= \rho^2 \left(2\sum_k \omega_k (\omega_k^2 \rho/\kappa - \kappa/\rho) E_k\right)^{1/2}. \end{aligned} \tag{12}$$

For large N, these quantities can be easily estimated: as for the ρ, for example, if the harmonic energies E_k (constants of motion) are independent of the frequencies ω_k:

$$\frac{1}{N}\sum_k \omega_k E_k \approx \frac{1}{N}\sum_k \omega_k \frac{1}{N}\sum_k E_k$$

i.e. the average of the product is approximately equal to the product of the averages. This occurs, for example, with uniform or random distributions $\{E_k\}$. In our models, with the

harmonic spectrum (8) and (10), the mean value of the ω_k rapidly tends to a limit value $\bar{\omega}$, independent of N, so that

$$\rho \approx E^{-1/2}(2\bar{\omega})^{-1/2}.$$

In the general case, this expression is multiplied by a correlation factor which depends only on the shapes of the two distributions $\{E_k\}$ and $\{\omega_k\}$. Similar estimates and considerations apply to κ and $|\tau|$, so that we may summarize the following properties of the quantities (12):

- they behave as $E^{-1/2}$;
- harmonic energy distributions independent of the spectrum give the same value for them;
- when normalized through $E^{-1/2}$, they depend only on the correlation between the harmonic energies and the spectrum;
- when normalized as before, they are not affected by the linear rescaling of the harmonic energies, even in case of correlation.

As for the anharmonic Hamiltonians $H = H_0 + V'$, we consider the quartic Fermi–Pasta–Ulam model with periodic boundary conditions, and the Lennard–Jones model with fixed boundary conditions. The FPU system is characterized by the anharmonic potential

$$\varepsilon V_4(\boldsymbol{x}) = \frac{\varepsilon}{4}\sum_{i=1}^{N}(x_i - x_{i+1})^4 \qquad (x_1 = x_{N+1}) \tag{13}$$

while the global potential (including the quadratic part) of the LJ system is

$$V_{LJ} = 4\hat{\varepsilon}\sum_{i=0}^{N}\left[\left(\frac{\sigma}{x_i - x_{i+1} + x_{eq}}\right)^{12} - \left(\frac{\sigma}{x_i - x_{i+1} + x_{eq}}\right)^{6}\right] + (N+1)\varepsilon \qquad (x_0 = x_{N+1} = 0). \tag{14}$$

In the last formula $x_{eq} = 2^{1/6}\sigma$ is the minimum of the potential well, and the $\{x_i\}$ are the deviations from the equilibrium positions $i \cdot x_{eq}$ of the ith particle. A power series expansion gives the quadratic potential as in (6) with $\chi = 9 \cdot 2^{8/3}\hat{\varepsilon}/\sigma^2$.

For comparisons with previous experiments, the parameters have been taken at the following fixed values: $\varepsilon = 0.1$ and $\chi = 1$ in FPU, $\hat{\varepsilon} = 27.5$ and $\sigma = 1$ in LJ. We shall see that with these parameters the thresholds are localized at close values of the specific energy u for both systems.

We shall examine also systems obtained by varying some conditions. For instance, the quartic FPU model with fixed boundaries, or the FPU model including also the third-order potential

$$V_3 = \eta\sum_{i=0}^{N}(x_i - x_{i+1})^3 \tag{15}$$

with η ranging from 0 up to the value of ε, i.e. 0.1.

Finally, for comparison with an integrable model, we shall consider the Toda chain whose potential is

$$V_T = \alpha\sum_{i=0}^{N}(\mathrm{e}^{-\beta(x_i - x_{i+1})} + \gamma(x_i - x_{i+1})). \tag{16}$$

where $\beta = -2^{-1/6}$, $\gamma = \mathrm{e}\beta$ and $\alpha = 3.76$. These values for β and γ are obtained by fixing position and value of the minimum as for V_{LJ}, while α has been chosen in order to localize the onset of anharmonicity approximately at the same value of u as in the other models.

4. Numerical experiments and results

Experiments have been performed by varying the number N of degrees of freedom from 32 to 4096. As usual, for comparisons at different N, we study our variables as functions of the specific energy $u = E/N$, from 10^{-4} to 30, with several checks below and above this range. The integration routine (a standard fifth order Runge–Kutta) required integration steps different for the FPU and the LJ systems, and different at different energies. The step sizes were always chosen to ensure a very good energy conservation (one part over 10^7 in the worst case).

The typical total elongation of the trajectories was given by 600 of the shortest harmonic periods, and the samplings for the averages by 4000 instantaneous values. Several checks up to 2400 periods have been performed. Experiments on the time behaviour, in order to examine the dependence on the initial conditions, reached 16 000 periods.

The initial conditions have been chosen randomly for the variables $\{\boldsymbol{x}, \dot{\boldsymbol{x}}\}$ or $\{\hat{\boldsymbol{p}}, \hat{\boldsymbol{q}}\}$. This means that the initial harmonic energies E_k were slightly correlated to the frequencies ω_k, so that the quantities (12) in the harmonic model were also slightly dependent on the initial conditions, even at very high N. The actual choice, 'democratic' but sufficient to give evidence to the role of the initial conditions, requires some care in order to compare the anharmonic experiments at different energies: specifically, the initial $\{E_k\}$ distribution must keep constant the reference harmonic case. Therefore, the correct way to increase the specific energy is obtained by assuming the same random choice for $\{\hat{\boldsymbol{p}}, \hat{\boldsymbol{q}}\}$ (or $\{\boldsymbol{x}, \dot{\boldsymbol{x}}\}$), with a linear scaling of the harmonic energies E_k through the scaling of the coordinates. This corresponds to follow a 'radius' in the phase space, i.e. to cross the different constant energy surfaces along a fixed direction. Several experiments have been performed by following different radii.

First, we distinguish the results referring to time averages from those referring to their variances.

4.1. Time averages

For simplicity we shall use for them the symbols ρ, κ, τ and ρ_n, κ_n, τ_n.

4.1.1. FPU. The plots for ρ, κ and τ are reported in figure 1. At low energies they all keep approximately the same values as in the harmonic system with the same initial conditions. Due to the log–log scale, a certain care is required for κ and ρ in order to grasp where the deviations from the harmonic behaviour (slope $-\frac{1}{2}$) start. It is clear, anyway, that ρ deviates to a steeper slope whereas κ and τ deviate to an easier one. This fact stresses the advantage of normalizing curvature and torsion by the microcanonical density, as in (5).

Figure 2 shows the normalized quantities obtained by following five different radii in the phase space. The factor $A = 2$ in the normalization (4) has been chosen just to avoid the overlapping of ρ_n and τ_n. As expected, all the plotted quantities exhibit a sharper behaviour than those of figure 1. For every fixed radius, the dependence on u below the transition can be directly related to the quasi-harmonicity of the system, in the sense that the mean values are almost exactly the harmonic values, while at high energy such a correspondence disappears. The dependence on the initial conditions is clearly displayed for low energy, while at high energy the five lines become undistinguishable. Such a behaviour may be directly read in terms of the Birkhoff theorem: the vanishing dependence on the initial conditions characterizes the transition interval around a threshold specific energy $\tilde{u}$ as the transition from nonergodic to ergodic regime of motion. Figures 3 and 4 show, for instance,

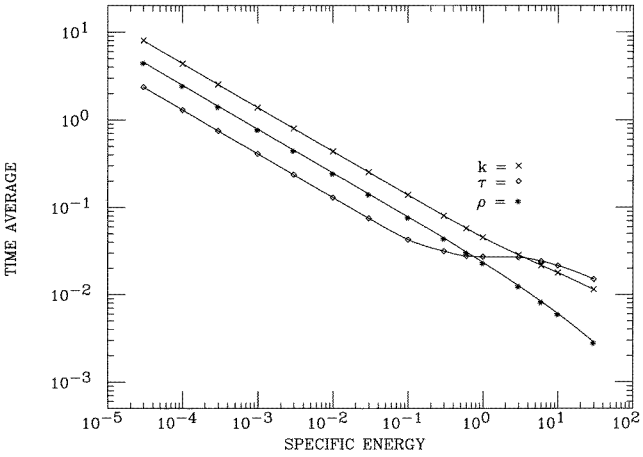

Figure 1. Plots of time averaged κ, τ and ρ versus u, for the FPU model with $N = 512$. Total integration time corresponds to 600 of the shortest harmonic periods. The averages run over 4000 instantaneous values.

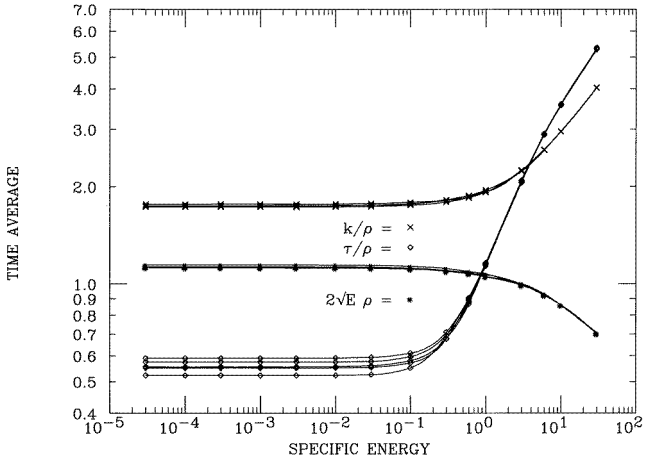

Figure 2. Plots of time averaged κ_n, τ_n and ρ_n versus u, for initial conditions along five different radii in the FPU model. Other parameters are as in figure 1.

the time dependence of κ_n below and above threshold for four initial conditions. Actually, the latter are chosen differently from those in the previous figure to give better evidence of the spread of values.

The observables ρ_n and κ_n retain the harmonic value up $u = 0.1$, and τ_n up to $u = 0.03$. This small difference will be regularly noted in all the experiments. The threshold specific energy $\tilde{u}$ defined by these values is within the estimates obtained through other stochastic parameters and criteria, such as equipartition, spectral entropy and Lyapunov exponents. We remark on the definiteness of the left bounds of transition interval in figure 2. Furthermore, the stability of these bounds is reached early in time, i.e. within 600 of the shortest periods, which usually are not sufficient with other approaches to get similar reliability. Checks up to 2400 periods have been performed. From a general point of view, this could imply that the quasi-harmonic (respectively, non-harmonic) features of the trajectories are nearly

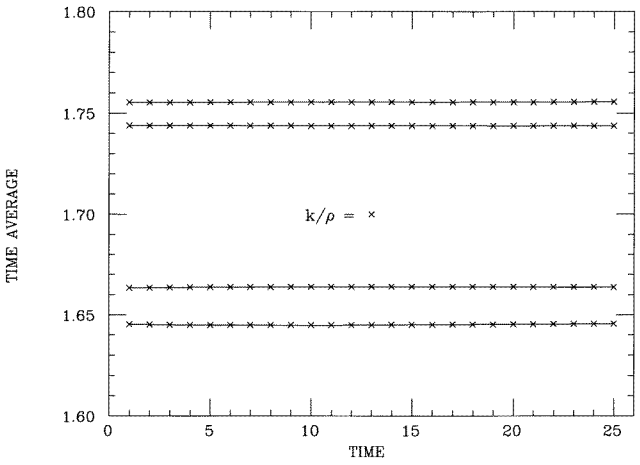

Figure 3. Time behaviour of the averaged κ_n for four initial conditions below the harmonicity threshold ($u = 0.01$) in the FPU model. The final time corresponds to 600 of the shortest harmonic periods.

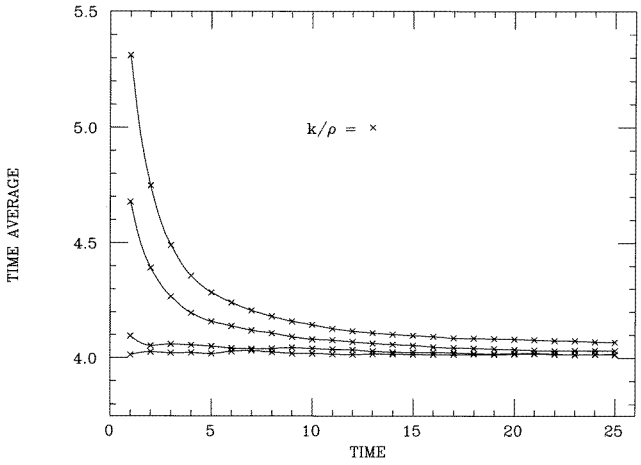

Figure 4. Time behaviour of the averaged κ_n for four initial conditions (the same as in figure 3, rescaled) above the harmonicity threshold ($u = 30$) in the FPU model. Final time as in figure 3.

steady properties all over the evolution, so that they may be immediately estimated without long relaxation times.

4.1.2. LJ. Qualitatively, nothing changes with respect to FPU, at least for the stochastic transition. We only mention a certain numerical instability of the results at high energy. Figure 5 shows the analogous figure 2 for a single radius in the phase space. The factor $A = 1000$ in the normalization (4) for ρ_n has been chosen to obtain the same order of magnitude as for κ_n and τ_n. We omit to reproduce figures corresponding to figures 3 and 4 since they are equivalent apart from the time scale: the LJ model seems indeed to be much slower in the approach to equilibrium. However, the time required to establish the stable bounds in u as given by figure 5 is the same as for FPU.

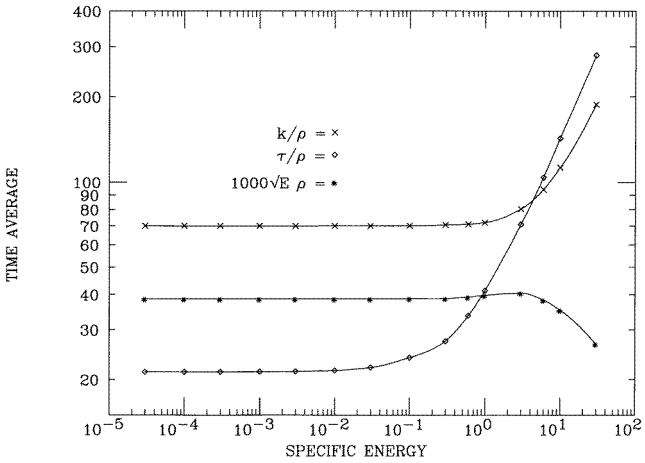

Figure 5. Plots of κ_n, τ_n and ρ_n, corresponding to those of figure 2, for a single radius, in the LJ model. Degrees of freedom and calculation parameters as in figure 1.

4.1.3. For a comparison with an integrable model, we also examine the Toda chain (see equation (16)). By choosing the parameters as in section 3, the plots corresponding for instance to those in figure 2 exhibit a similar transition to non harmonic behaviour at the same specific energy. However, as shown for the curvature in figure 7, the diagrams for different radii remain distinguishable also above the transition. As expected, below and above this non-harmonicity threshold the time plots (that we omit) are similar, and both are similar to those in figure 3: in other terms, at all energies there is a time stable dependence on the initial conditions.

4.2. Variances

4.2.1. FPU. As said before, in most cases the variances of κ, τ and ρ have been calculated over 4000 instantaneous values along the orbit, a number that is still not sufficient for good stabilization in the stochastic regime, but it is largely sufficient to localize a transition. This transition, which individuates the same interval in u previously observed in figures 1 and 2, consists in a neat breakdown of the linear growth, with slope very close to 2, in the log–log diagrams (see figure 6). Differently from the case of mean values, a direct comparison with the harmonic value (identically 0) is meaningless.

4.2.2. LJ system. The stability is in general worse than in the FPU case, especially at high energy, inasmuch as the indication of the transition. However, a good estimate of the slope in the ordered region is still possible, and gives a value close to 1 (figure 8).

4.3. Dependence on N

With N from 32 to 4096, the transition specific energy $\tilde{u}$ shows remarkable stability, for both FPU and LJ systems. Figure 9, for $N = 4096$, overlaps figure 1, for $N = 512$, apart from a shift down, while figure 10, referring to normalized quantities, is practically identical to figure 2 over the full range of specific energy. By recalling that ρ_n is normalized with $E^{-1/2} = u^{-1/2}N^{-1/2}$, and κ_n and τ_n are normalized with ρ, this overlapping shows that ρ, κ and τ depend on N only through the factorized function $N^{-1/2}$. Below threshold, this is

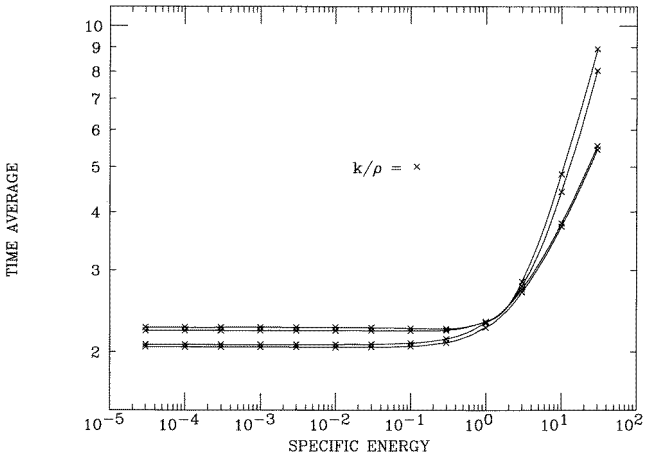

Figure 6. Plots of κ_n versus u with initial conditions along four radii for the Toda model. Degrees of freedom and other parameters as in figure 1.

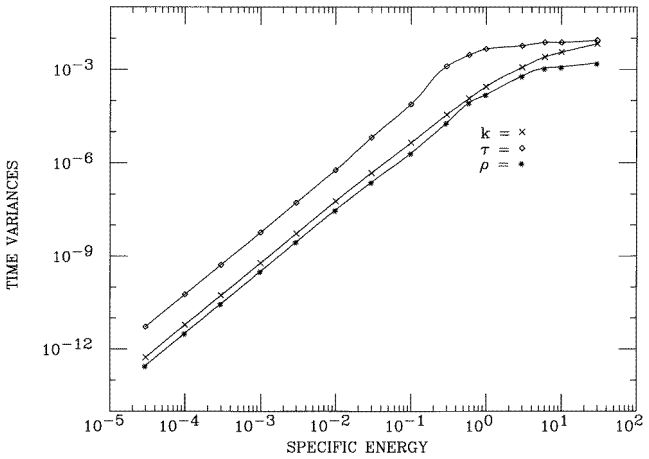

Figure 7. Variances computed along the same orbits as in figure 1, in the FPU model for κ, τ and ρ versus u.

simply related to the quasi-harmonic behaviour $E^{-1/2}$ already observed after (12), whereas it represents a new result above threshold.

Also the variances are shifted down as N increases, but a similar procedure of normalization is not simply transferrable, because of the nonlinearity of the variance itself.

4.4. Main differences and comparisons

Thus the main difference between the two models consists in the slope of the variances in the quasi-harmonic regime, which behave as u^2 and u in the FPU and LJ systems, respectively. Actually, another difference between the two models has been found in the experiments. We have evaluated the averaged absolute derivatives, obtaining the same results for the

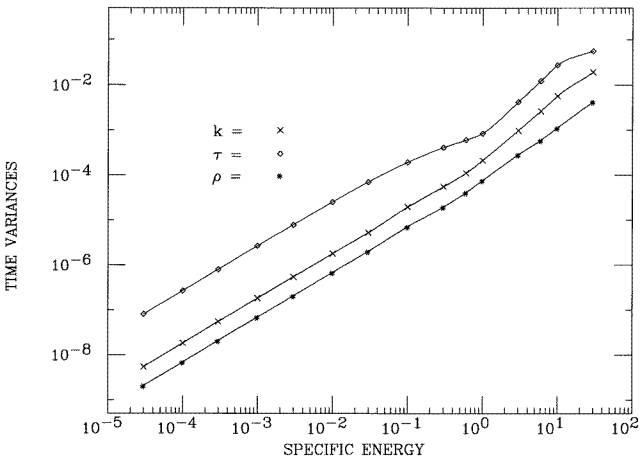

Figure 8. Variances corresponding to those of figure 7 for the LJ model. Values at high energies are not completely reliable.

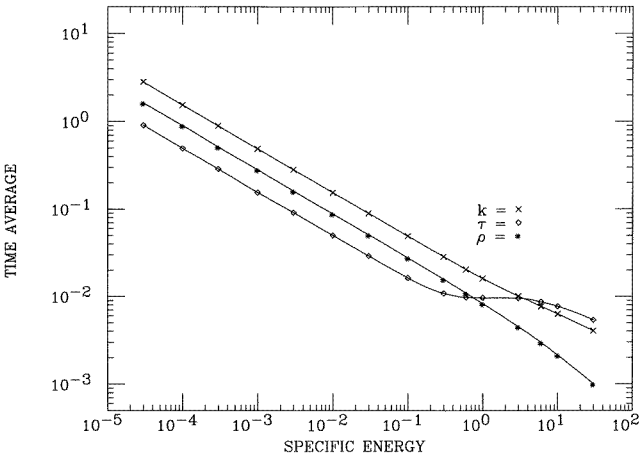

Figure 9. Plots corresponding to those of figure 1 for $N = 4096$. Note the vertical shift of the figure, and the overlapping of the transition interval.

three observables ρ, κ and τ, i.e.

$$\left\langle \left| \frac{\mathrm{d}f}{\mathrm{d}t} \right| \right\rangle \propto u^{1/2} \qquad \left\langle \left| \frac{\mathrm{d}f}{\mathrm{d}t} \right| \right\rangle \propto \text{constant} \tag{17}$$

for FPU and LJ systems, respectively.

From the behaviours of variances and derivatives, it is possible to draw some phenomenological consequences on the geometrical structure of the phase space. Let us first introduce the amplitude Δf of the fluctuation for every computed observable f, by using the definition (2):

$$\Delta f \equiv \sqrt{\langle f^2 \rangle - \langle f \rangle^2} = \langle f \rangle \sqrt{\mathrm{Var}(f)}. \tag{18}$$

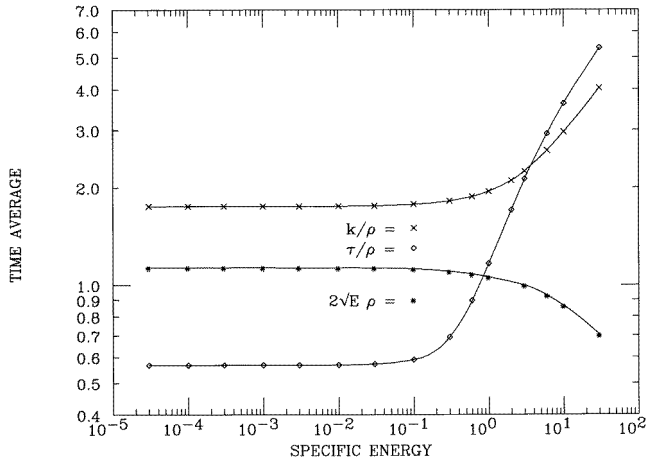

Figure 10. Plots corresponding to those of figure 2 for $N = 4096$, for a single radius. Note again the perfect overlap of the figure without any vertical shift.

Remembering that, for both systems, the averaged observables decrease as $u^{-1/2}$, from the behaviours of the variances we obtain

$$\Delta f \propto u^{1/2} \qquad \Delta f \propto \text{constant} \tag{19}$$

for FPU and LJ systems, respectively.

We may now introduce a 'frequency' for the observable f through the formula

$$\nu(f) \approx \frac{\langle |\mathrm{d}f/\mathrm{d}t| \rangle}{4\Delta f}. \tag{20}$$

For a regularly oscillating phenomenon, expression (20) would represent the proper frequency. Therefore, in our case, this definition is a reasonable one on the basis of the usual assumption, i.e. that in the ordered regime of motion the trajectories oscillate almost regularly, in the mean, around their harmonic counterparts at the same energy. This assumption, besides its general consistency with our results, has been well confirmed by direct checks.

Therefore, from (17), (19) and (20) we obtain

$$\langle \nu(f) \rangle \propto \text{constant} \tag{21}$$

for both the systems in the whole ordered range. The same quantity multiplied by ρ, the mean of the inverse absolute velocity (see (3)), represents the mean wave number $\langle n(f) \rangle$, with the following dependence on u:

$$\langle n(f) \rangle \propto u^{-1/2}. \tag{22}$$

These considerations, summarized in table 1, provide information about the way in which the phase point moves on the deformed invariant surface.

4.5. Further checks on other systems

A series of checks have proven that the boundary conditions have no influence, and that the qualitative differences between FPU and LJ systems exclusively depend on the presence/absence of the third-order term in the Hamiltonian. More precisely, this means that including the cubic interaction (15) with coefficient η in the FPU model, the variances

Table 1. Behaviour versus u, in the ordered regime, of different quantities related to three observables ρ, κ and τ (indicated as f).

	FPU	LJ
$\langle f \rangle$	$\propto u^{-1/2}$	$\propto u^{-1/2}$
$\mathrm{Var}(f)$	$\propto u^{2}$	$\propto u$
$\Delta(f)$	$\propto u^{/2}$	$\propto$ constant
$\langle \lvert \mathrm{d}f/\mathrm{d}t \rvert \rangle$	$\propto u^{1/2}$	$\propto$ constant
$\langle \nu(f) \rangle$	$\propto$ constant	$\propto$ constant
$\langle n(f) \rangle$	$\propto u^{-1/2}$	$\propto u^{-1/2}$

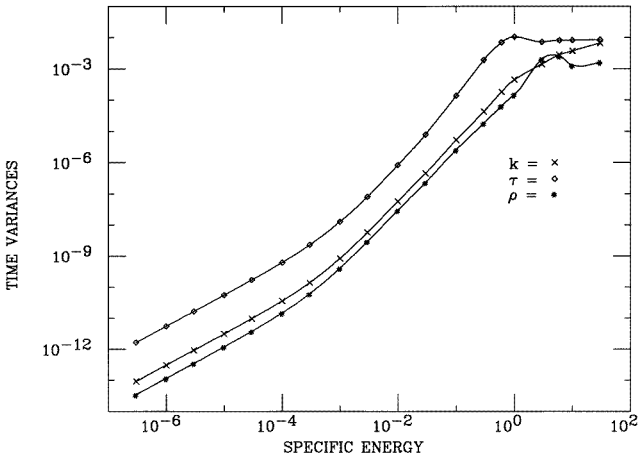

Figure 11. Plots of the variances, corresponding to those of figures 7 and 8, for the modified FPU model including a cubic interaction with a coefficient $\eta = 0.01$ giving evidence to the transition from the slope 1 to the slope 2.

and the time derivatives undergo a transition from the standard FPU behaviour to the LJ behaviour, when η goes from 0 to the magnitude of ε (provided that the energy is not too small). Figure 11, referring to the variances of the model with coefficient $\eta = 0.01$, exhibits indeed a transition from the slope 1 at very low energies, where the cubic term is always dominant, to slope 2, where the coefficient η makes the cubic term negligible with respect to the quartic one.

For all these experiments, we exploited the computing facilities at the University of Parma: Digital Alfa, VAX 7090 and Thinking Machine CM2.

5. Conclusions

There are two kind of conclusions, referring, respectively, to the efficiency of the new parameters as stochastic indicators and to the possibility they offer of a deeper insight into the phenomena of transition. Actually, by testing them on integrable and non-integrable systems, we found that these quantities sharply indicate the passage from a harmonic-like behaviour to a non-harmonic one. Furthermore, they also prove to be sensitive to the initial conditions, so that, in the perspective of the Birkhoff theorem, they are able to distinguish ergodic from non-ergodic behaviour. The transition indicated by these parameters occurs at the same energies given by other stochastic parameters as Lyapunov exponents, or equipartition

based indicators.

Moreover, their very definition has the desired property of testing the geometrical structure of the phase space (presence/absence of invariant surfaces) in a way that is largely independent of N and substantially faster than the indicators related to the approach to equilibrium. This method has the further advantage of a great numerical definiteness. It is particularly noteworthy that, with N growing from 32 to 4096, the stochastic threshold remains practically stable, as proven by the perfect overlapping between figures 2 and 10 (referring to $N = 512$ and $N = 4096$, respectively). The numerical evidence about the persistence of a threshold independent of N is extremely good and perfectly consistent with the analytical estimates obtained by [6] and [9] for the SST with other methods. Remaining within our conceptual frame, we stress the last considerations in section 4, about the possibility of looking at certain regularities in the oscillations of the trajectories around their harmonic counterparts at low energies. They prove that it is possible to have information concerning the way the invariant surfaces, before vanishing, are deformed. For instance, now we know that the third-order term in the potential has a remarkable influence on the oscillations around the mean harmonic values, and consequently on their amplitudes, while the roughly defined frequencies of such oscillations are independent of u.

We shall discuss in a forthcoming paper the analytical derivations of such behaviour, and the possibility that the geometric properties of the trajectories we started to analyse contain more detailed information about the differential features of the invariant surfaces. In this context, the systematic small differences between transition values actually present in κ and τ could receive meaningful interpretation.

Acknowledgment

We thank A Scotti for helpful discussions.

References

[1] Benettin G, Galgani L and Strelcyn J M 1976 *Phys. Rev.* A **14** 2338
[2] Alabiso C, Casartelli M and Marenzoni P 1993 *Phys. Lett.* **183A** 305
[3] Alabiso C, Casartelli M and Marenzoni P 1995 *J. Stat. Phys.* **79** 451–71
[4] De Luca J, Lichtenberg A J and Lieberman M A 1994 Time scale to ergodicity in the Fermi–Pasta–Ulam system *Preprint* University of California, Berkeley
[5] Kantz H, Livi R and Ruffo S 1994 *J. Stat. Phys.* **76** 627–43
[6] Casetti L, Livi R and Pettini M 1995 *Phys. Rev. Lett.* **74** 375
[7] Casartelli M and Sello S 1987 *Nuovo Cimento* B **97** 183; 1985 *Phys. Lett.* **112A** 249; 1987 *Advances in Nonlinear Dynamics and Stochastic Processes—II* ed G Paladin and A Vulpiani (Singapore: World Scientific)
[8] Pettini M 1993 *Phys. Rev.* E **47** 828
[9] Casetti L and Pettini M 1993 *Phys. Rev.* E **48** 4320
[10] Pettini M and Valdettaro R 1995 *Chaos* **5** 646